

The Structure and Dynamic Instability of Isothermal Relativistic Star Clusters

Edward D. Fackerell and Kevin G. Suffern

Department of Applied Mathematics, University of Sydney, Sydney, N.S.W. 2006.

Abstract

The structure and dynamic stability of isothermal relativistic star clusters are discussed both for the case of clusters without dispersion in stellar rest mass and for two families of clusters with dispersion in stellar rest mass. We show that the former are dynamically unstable if the central redshift is greater than about 0·5, and that the latter are dynamically unstable if the central redshift is greater than about 0·6, so that the inclusion of dispersion in mass does not greatly affect the stability of isothermal relativistic star clusters.

1. Introduction

In this paper we present a detailed discussion of the structure and dynamic instability of spherically symmetric isothermal relativistic star clusters. Such clusters have isotropic velocity distributions and truncated Maxwell–Boltzmann distributions in energy. We study two distinct classes of these clusters in this paper: (a) in which there is no dispersion in the stellar rest mass; (b) in which there is dispersion in the stellar rest mass. For brevity we refer to the clusters with no dispersion as ND clusters, and to those with dispersion as D clusters.

The structure of ND clusters was first studied by Zeldovich and Podurets (1965), and independently by Fackerell (1966). Their dynamic stability was first investigated by Ipser (1969) who developed a variational principle for small radial pulsations of relativistic star clusters. The specific isothermal clusters that Ipser studied were dynamically unstable if the redshift of a photon emitted at the cluster's centre and received at infinity (the central redshift z_c) satisfied $z_c \gtrsim 0\cdot55$. More recently, Katz *et al.* (1975) (hereafter referred as KHK) studied the *thermodynamic* stability of ND clusters and reported the existence of two zones of parameter space where these clusters might be thermodynamically stable. Since their conditions were only necessary for thermodynamic stability, and not sufficient, KHK did not prove that any particular clusters were thermodynamically stable. The structure of D clusters was first studied by Fackerell (1966) and later generalized by Suffern (1976).

Since Ipser (1969) only studied certain sequences of ND clusters, and because it is important to discover whether any ND clusters could be both dynamically stable and thermodynamically stable, we have made a detailed study of the dynamic stability of these clusters. We have also studied the dynamic stability of D clusters in their generalized form. The method we use is a refinement of Ipser's variational principle

which gives a simple sufficient condition for dynamic instability. This refinement was devised by Fackerell (1970, hereafter referred to as Paper I). Although our results for ND clusters have been published elsewhere (Suffern and Fackerell 1976), no details of the calculations were given in that paper. Some of these results are repeated here for completeness and for direct comparison with the corresponding results for D clusters. Section 2 presents the theory and structure of isothermal clusters, Section 3 describes the method for diagnosing dynamic instability, Section 4 discusses the numerical techniques used and Section 5 presents and discusses the results.

2. Theory and Structure of Isothermal Clusters

Throughout the paper we use gravitational units in which $G = c = k = 1$, and we describe the clusters in terms of the spherical line element

$$ds^2 = \exp(\nu) dt^2 - \exp(\lambda) dr^2 - r^2 \{d\theta^2 + \sin^2(\theta) d\phi^2\}.$$

Distribution Functions

Isothermal relativistic star clusters are characterized by distribution functions of the form

$$F(m, E) = g(m) H(E_{\max} - E) \exp(-E/m_0 T_\infty). \quad (1)$$

Here $g(m)$ is an arbitrary function of the stellar rest mass, m_0 is a reference stellar rest mass, H is the Heaviside step function, E is the conserved energy along a stellar trajectory and T_∞ is the global temperature per unit stellar rest mass. Both E and T_∞ are values as measured by an infinitely removed observer. In addition, E_{\max} is a cutoff energy which guarantees that all the stars are confined to a finite region of space, since clusters with Maxwell-Boltzmann distributions in energy have infinite radii and masses unless the energy tail is truncated at some finite value.

For the two classes of clusters under consideration here, $g(m)$ is defined as follows:

For ND clusters

$$g(m) = Km_0^{-4} \delta(m - m_0), \quad (2)$$

where K is a constant, and δ is the Dirac delta function.

For D clusters

$$g(m) = \{K/\Gamma(\alpha)\} m_0^{-5} (m/m_0)^{\alpha-5} \exp(-\gamma m/m_0), \quad (3)$$

where α and γ are positive constants.*

These choices for $g(m)$ have been made largely for reasons of mathematical convenience, and not for any intrinsic physical reason, apart from supplying an example with dispersion in mass. The extent to which $g(m)$ in equation (3) is affected by varying α and γ is discussed in Section 5.

* Fackerell (1966) only considered the case with $\gamma = 1$.

Integral Expressions for p , ρ and ρ_0

For isotropic clusters we may define a mass-weighted distribution function (Fackerell 1966, 1970)

$$\chi(x) = \frac{2}{3}\pi \int_0^\infty F(m, m\beta^{\frac{1}{2}}x^{\frac{1}{2}}) m^4 dm, \quad (4)$$

where $x = E^2/m^2\beta$, and β is the value of the metric function $\exp(v)$ at the boundary of the cluster. If R is the coordinate radius of the boundary then we have $\beta = \exp\{v(R)\}$, and the cutoff energy is $E_{\max} = m\beta^{\frac{1}{2}}$. This guarantees that no stars are found at $r > R$ (Ipser 1969) and restricts the variable x to $x \leq 1$.

If we define $y = \exp\{v(R)\}/\beta$ then, in terms of $\chi(x)$, the pressure p , density of mass-energy ρ and density of rest mass ρ_0 are given by the following integral expressions (Paper I)

$$p = y^{-2} \int_y^1 \chi(x) x^{-1/2} (x-y)^{3/2} dx, \quad (5)$$

$$\rho = 3y^{-2} \int_y^1 \chi(x) x^{1/2} (x-y)^{1/2} dx, \quad (6)$$

$$\rho_0 = 3y^{-3/2} \int_y^1 \chi(x) (x-y)^{1/2} dx. \quad (7)$$

For $g(m)$ given by equations (2) and (3), the Appendix (below) discusses the evaluation of p , ρ and ρ_0 in terms of hypergeometric functions.

Structure Equations

To write the equations of structure in a suitable dimensionless form we follow Fackerell's (1966) procedure:

(1) We introduce a dimensionless radial coordinate $\xi = r/L$, where $L = (p_c/4\pi\rho_c^2)^{\frac{1}{2}}$ is a scaling parameter with dimensions of length. Here p_c and ρ_c denote the values of the pressure and density at the centre of the cluster, $r = 0$.

(2) We introduce a dimensionless mass function $v = M(r)/(L\sigma)$, where $\sigma = p_c/\rho_c$, and $M(r)$ is the total mass-energy inside a sphere of radius r .

(3) We introduce a dimensionless rest mass function $w = M_0(r)/(L\sigma)$, where $M_0(r)$ is the total rest mass contained within a sphere of radius r .

The field equations for the equilibrium structure of the clusters now take the form (cf. Ipser 1969)

$$dy/d\xi = 2\sigma y(v\xi^{-2} + \sigma\xi p/p_c) \exp(\lambda), \quad dv/d\xi = \xi^2 \rho/\rho_c, \quad dw/d\xi = \xi^2 \exp(\frac{1}{2}\lambda) \rho_0/\rho_c, \quad (8a, b, c)$$

with

$$\exp(\lambda) = (1 - 2\sigma v/\xi)^{-1}. \quad (9)$$

The equations (8a)–(8c) are integrated from the centre $\xi = 0$, at which $v = 0$, $w = 0$ and $y = y_c < 1$ (for y_c specified), to the boundary $\xi = \xi_1$, at which y is unity. The solution of these equations is further discussed in Section 4.

3. Stability Theory

The sufficient condition for dynamic instability of relativistic star clusters developed in Paper I depends upon the solution of the following single second-order ordinary differential equation of Sturm–Liouville type (cf. Paper I, equation 32):

$$\left(\xi^4 U(\xi) \exp(\frac{1}{2}\lambda) y^{3/2} \psi'(\xi) \right)' - \xi^2 \exp(\frac{1}{2}\lambda) y^{3/2} \left[\left(\frac{p}{p_c} + \frac{\rho}{\sigma \rho_c} \right) \left\{ \frac{3\xi y'}{2y} - \left(\frac{\xi y'}{2} \right)^2 + 1 - \exp(\lambda) \right\} y^{-1} + U(\xi) \left\{ \frac{1}{2} \left(\frac{\xi y'}{y} \right)^2 - \frac{5\xi y'}{6y} - \frac{2\sigma \exp(\lambda)}{3} \left(\frac{\xi^2 \rho}{\rho_c} - \frac{v}{\xi} \right) + \frac{\sigma \xi y' \exp(\lambda)}{y} \left(\frac{\xi^2 \rho}{\rho_c} - \frac{v}{\xi} \right) + 1 - \exp(\lambda) \right\} \right] \psi(\xi) = 0. \quad (10)$$

Here a prime denotes differentiation with respect to ξ , the function $\psi(\xi)$ is a trial function associated with Ipser’s (1969) variational principle, and $U(\xi)$ is the following phase space integral

$$U(\xi) = -(6/5y^3 p_c) \int_y^1 \dot{\chi}(x) x^{-1/2} (x-y)^{5/2} dx, \quad (11)$$

so that we have $U = \beta J_{-1,4}/p_c$ in the notation of Paper I, equation (A7). It follows from equation (4) that $\dot{\chi}$ ($= d\chi/dx$) is given by

$$\dot{\chi}(x) = \frac{1}{3} \pi \beta^{1/2} x^{-1/2} \int_0^\infty F_E(m, m\beta^{1/2} x^{1/2}) m^5 dm, \quad (12)$$

where F_E (which is negative) denotes $\partial F(m, E)/\partial E$ at constant m .

To diagnose dynamic instability in a relativistic star cluster, equation (10) is integrated from $\xi = 0$, with boundary conditions $\psi(0) = 1$ and $\psi'(0) = 0$, to the boundary of the cluster $\xi = \xi_1$. According to the theory outlined in Paper I, a sufficient condition for the cluster to be dynamically unstable against small radial pulsations is that ψ has a node somewhere inside the cluster. We now derive integral expressions for $U(\xi)$ when $g(m)$ has the forms (2) and (3), and the numerical evaluation of $U(\xi)$ is then discussed in the next section.

For ND clusters, it follows from equations (1), (2) and (12) that

$$\dot{\chi}(x) = -\frac{1}{12} \pi K x^{-\frac{1}{2}} \{ \mu H(1-x^{\frac{1}{2}}) + \delta(1-x^{\frac{1}{2}}) \} \exp(-\mu x^{\frac{1}{2}}), \quad (13)$$

where for computational convenience (see Section 4 below) we have introduced the parameter $\mu = \beta^{\frac{1}{2}}/T_\infty$. Consequently $U(\xi)$ follows from equation (11) as

$$U(\xi) = \frac{\pi K \exp(-\mu)}{5y^3 p_c} \left((1-y)^{5/2} + \mu Y^{7/2} Z^{5/2} \int_0^1 \frac{(1-u)^{5/2} (1-Yu/Z)^{5/2} \exp(\mu Yu) du}{1-Yu} \right), \quad (14)$$

where $Y = 1-y^{\frac{1}{2}}$ and $Z = 1+y^{\frac{1}{2}}$.

For D clusters it similarly follows that

$$\dot{\chi}(x) = -\frac{1}{12}\pi K x^{-\frac{1}{2}}(\gamma + \mu x^{\frac{1}{2}})^{-(\alpha+1)}\{\mu\alpha H(1-x^{\frac{1}{2}}) + (\gamma + \mu x^{\frac{1}{2}})\delta(1-x^{\frac{1}{2}})\}, \quad (15)$$

and consequently that

$$U(\xi) = \frac{\pi K(\gamma + \mu)^{-(\alpha+1)}}{5y^3 p_c} \left((\gamma + \mu)(1-y)^{5/2} + \mu\alpha Y^{7/2} Z^{5/2} \int_0^1 \frac{(1-u)^{5/2}(1-Yu/Z)^{5/2}\{1-\mu Yu/(\gamma + \mu)\}^{-(\alpha+1)} du}{1-Yu} \right). \quad (16)$$

4. Solution of Equations

Since the equations of structure (8a)–(8c) contain only the ratios p/p_c , ρ/ρ_c and ρ_0/ρ_c , they do not involve the constants K and m_0 which appear in equations (2) and (3). Consequently, these constants do not affect the *dimensionless* structure of the isothermal clusters. In dimensionless form, the ND clusters form a two-parameter set and, although several choices of parameters are possible, there is one pair which is most suitable from a computational point of view: y_c , the value of y at the cluster centre, and μ . It is shown in the Appendix that the equilibrium values of p , ρ and ρ_0 are most conveniently expressed in terms of μ . The situation for the D clusters is similar, except that they form a four-parameter sequence, where the constants α and γ in equation (3) are the two extra parameters.

The value of y_c is used as the central boundary condition in equation (8a) and, although the equations of structure in dimensionless form do not contain β , all dimensionless properties of ND clusters are uniquely determined once y_c and μ are specified. The same applies to D clusters when α and γ also are specified. Two properties of particular importance are the central redshift $z_c = (\beta/y_c)^{\frac{1}{2}} - 1$ and the global temperature $T_\infty = \beta^{\frac{1}{2}}/\mu$. It should be noted that β is unknown before the structure of a cluster is completely determined. But once the structure is calculated, it follows from equation (9) that

$$\beta = 1 - 2\sigma v(\xi_1)/\xi_1,$$

where $\exp(v) = \exp(-\lambda)$ at the surface of the cluster.

Another important dimensionless property of the cluster is the fractional binding energy \mathcal{E} defined by

$$\mathcal{E} = (M_0 - M)/M_0,$$

where M and M_0 are respectively the total mass–energy and total rest mass of the cluster. Since these quantities are given by $M = L\sigma v(\xi_1)$ and $M_0 = L\sigma w(\xi_1)$, it follows that

$$\mathcal{E} = 1 - v(\xi_1)/w(\xi_1). \quad (17)$$

Three additional properties are the ratio

$$M/R = \sigma v(\xi_1)/\xi_1, \quad (18)$$

the central condensation in the mass–energy density

$$\rho_c/\langle\rho\rangle = \xi_1^3/3v(\xi_1)$$

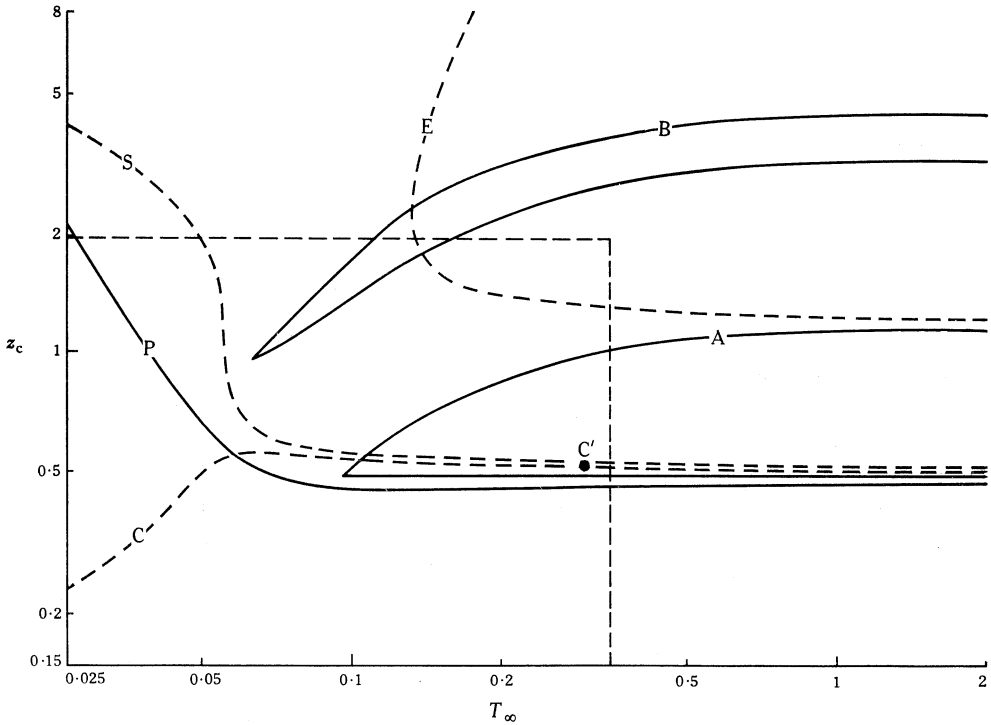


Fig. 1. Curves relating to dynamic instability of ND isothermal clusters in the z_c, T_∞ plane. All clusters above the dashed curve S are dynamically unstable. The full curves A and B enclose areas of possible thermodynamic stability discussed by KHK, while the dashed curves C and E denote respectively the locii of maximal fractional binding energy and zero binding energy. Ipser's (1969) variational principle for the squared frequencies of radial vibration of star clusters becomes positive definite below the full curve P for the particular form of trial function employed in this paper. For the area contained within the dashed rectangle, the binding energy is depicted in Fig. 2. The dot labelled C' on curve C is the position of the cluster upon which Fig. 6 (below) is based.

and the rest mass density

$$\rho_{0c}/\langle\rho_0\rangle = \xi_1^3/3w(\xi_1), \tag{19}$$

where ρ_{0c} is the central value of ρ_0 . The quantities

$$\langle\rho\rangle = 3M/4\pi R^3 \quad \text{and} \quad \langle\rho_0\rangle = 3M_0/4\pi R^3$$

are average densities taken over the coordinate volume of the cluster.

The phase space integral $U(\xi)$ is evaluated as follows: Since the integrals in equations (14) and (16) can be evaluated only in terms of hypergeometric functions of three independent variables (this contrasts with p, ρ and ρ_0 , which are evaluated in the Appendix below in terms of hypergeometric functions of two independent variables), they are most efficiently evaluated by numerical integration. Although a numerical technique such as Simpson's rule could be used at each integration step, it is more efficient from a computational point of view to use Simpson's rule only at the centre of the cluster where $y = y_c$. This gives the central value U_c of U , which can then be used as the boundary condition for solving the differential equation which U satisfies (equation (29) of Paper I), namely

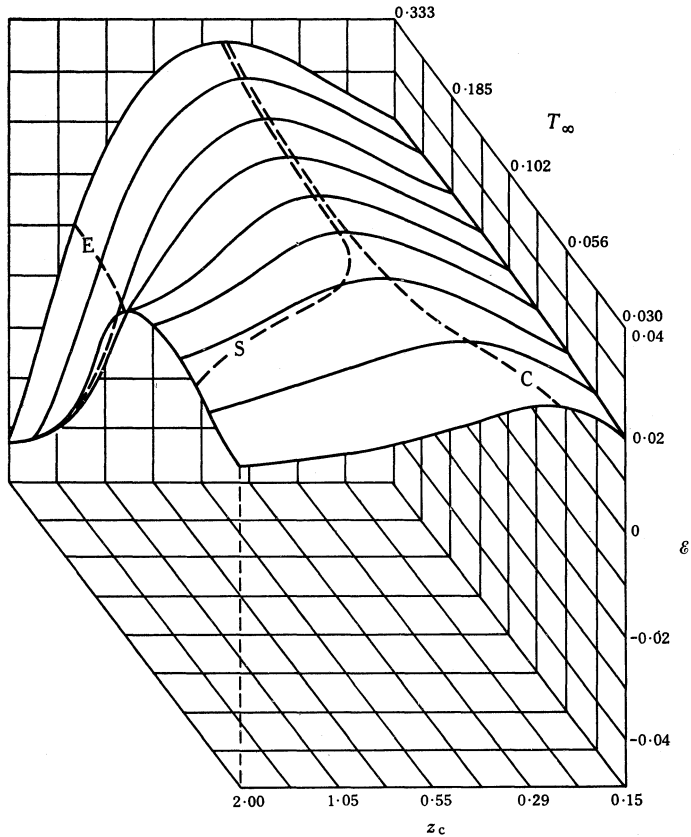


Fig. 2. Three-dimensional plot of the fractional binding energy \mathcal{E} for ND clusters over a section of the z_c, T_∞ plane. Marked on the surface are the following dashed curves: C along which \mathcal{E} has a local maximum; E along which \mathcal{E} is zero; the stability curve S.

$$\frac{dU}{d\xi} = -\frac{y'}{2y} \left\{ U + 3 \left(\frac{p}{p_c} + \frac{\rho}{\sigma\rho_c} \right) \right\}. \quad (20)$$

The differential equations of structure (8a)–(8c), the stability equation (10) and equation (20) for U were integrated together to determine the structure of the clusters and simultaneously to diagnose their dynamic instability. A fourth-order Runge–Kutta integration scheme was used, and at each integration step the values of p , ρ and ρ_0 were evaluated from the continued fraction expansions for the expressions (A2)–(A4) and (A11)–(A13) given in the Appendix. Since some clusters have extremely large coordinate radii ξ_1 , the variable of integration was changed from ξ to $1/\xi$ whenever $\xi = 10$ was reached.

5. Results and Discussion

ND Clusters

The results for ND clusters, obtained from the numerical calculations, are presented in Figs 1 and 2. A region of the z_c, T_∞ plane is shown in Fig. 1. The full curves labelled A and B in this figure enclose the two regions of possible thermodynamic stability discussed by KHK, while the dashed curve S is the locus of the onset of

dynamic instability as diagnosed by equation (10). For all the clusters tested which were located in the z_c, T_∞ plane above S, a node appeared in ψ before the boundary was reached and these clusters are thus dynamically unstable. The position of S in the plane was determined by the criterion that the node occurred at the boundary, and we are confident that we tested enough clusters above S to ensure that no regions of possible dynamic stability escaped our attention. Our confidence lies in the fact that, as the distance from S in the z_c, T_∞ plane increases, the node occurs relatively closer to the centre of the clusters, and does so monotonically with increasing distance from S.

As Fig. 1 indicates, all clusters in KHK's region B of thermodynamic stability are dynamically unstable, as are most of those in region A. The only ND clusters that could be both dynamically stable and thermodynamically stable are those lying in the thin strip above the lower part of A and below S. Since it is necessary for a cluster to be stable against all forms of instability if it is to have any chance of existing in nature, the only ND clusters that could exist would lie in this thin strip, unless other zones of thermodynamic stability exist with smaller central redshifts than those shown in Fig. 1.

The fractional binding energy \mathcal{E} as given by equation (17) has a local positive maximum along the dashed curve C, is zero along the dashed curve E and is negative above E. All dynamically stable clusters have positive binding energies, which is to be expected on physical grounds because any cluster with negative binding energy is energetically capable of dispersing itself to infinity if perturbed.

Fig. 2 shows the variation in \mathcal{E} over the portion of the z_c, T_∞ plane which is enclosed by the dashed rectangle in Fig. 1. For large values of T_∞ , the curves S and C are quite close, indicating that the onset of dynamic instability occurs close to the locus of maximum fractional binding energy. This agrees with previous stability studies of Ipser (1969), and its evolutionary significance was discussed by Fackerell *et al.* (1969). However, for temperatures below $T_\infty \approx 0.06$, the S and C curves rapidly diverge. This rapid divergence of S towards high values of z_c arises from the inability of Fackerell's method (Paper I) to diagnose instability in clusters with an extreme core-halo structure (i.e. clusters for which $\rho_c/\langle\rho\rangle \gtrsim 10^3$), which is the structure developed by ND clusters for low temperatures and high central redshifts (see Fig. 5 below). In fact, the clusters at the top left-hand corner of Fig. 1 have $\rho_c/\langle\rho\rangle \gtrsim 10^{13}$. The method of Paper I fails in these circumstances because it is based on Ipser's (1969) variational principle with the trial function approximated by the first term of an infinite series. The curve P, which also approaches high z_c for low T_∞ , is the locus of points at which the numerator integrand of Ipser's variational principle becomes positive definite when single-term trial functions are employed (see his equations 19 and 28). Such positive definite behaviour automatically excludes the possibility of a node occurring in ψ . However, for clusters that do not have core-halo structures the method is quite successful, and it is possible that the true dividing line in the z_c, T_∞ plane between dynamic stability and instability stays close to curve C for all values of T_∞ .

D Clusters

The additional parameters α and γ complicate the structural picture of D clusters to the extent that they require a double infinity of z_c, T_∞ planes for their complete specification. To simplify this picture somewhat we restrict attention here to two

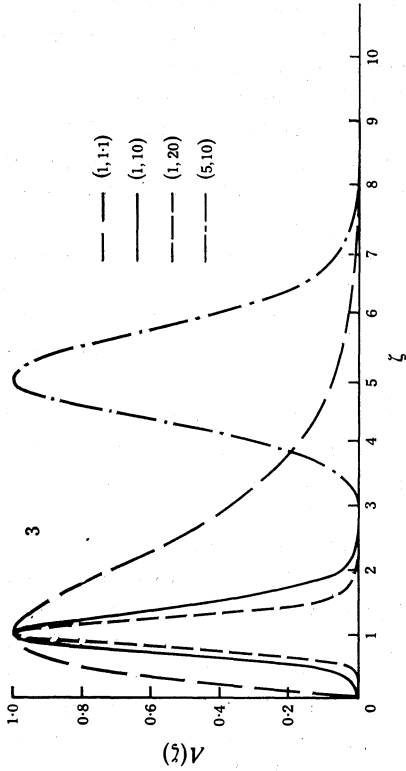
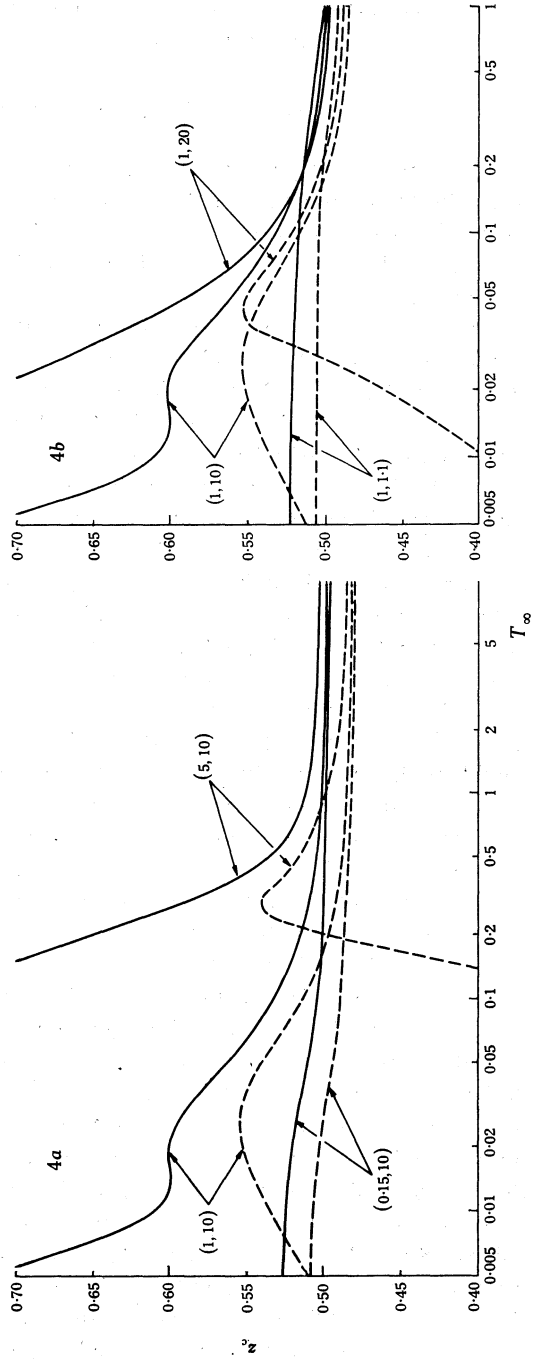


Fig. 3. The normalized rest mass distribution $A(z)$ of equation (21) for the indicated values of the parameters (n, γ) .

Fig. 4. Curves relating to dynamic instability of D clusters in the z, T_∞ plane for the indicated values of the parameters (n, γ) for : (a) clusters belonging to family [A], and (b) clusters belonging to family [B]. For each (n, γ) , all clusters in the z, T_∞ plane above the full curve are dynamically unstable, while \mathcal{E} has a local maximum along the dashed curve.



specific families of D clusters which together give a satisfactory amount of information about the complete parameter space.

If we define $\zeta = m/m_0$, the distribution in stellar rest mass $g(m)$ in equation (3) has a maximum at $\zeta = (\alpha - 5)/\gamma \equiv n$ and, by dividing $g(m)$ by its value g_{\max} at $\zeta = n$, we obtain the normalized distribution

$$A(\zeta) = g(\zeta)/g_{\max} = (\zeta/n)^{n\gamma} \exp\{-n\gamma(\zeta/n - 1)\}. \quad (21)$$

We now take n and γ as the two additional parameters instead of α and γ , and only study distributions with n and γ satisfying $\gamma > n^{-1}$, in order to avoid $A(\zeta)$ having an infinite derivative with respect to ζ at $\zeta = 0$. For a given n , the peak in $A(\zeta)$ about $\zeta = n$ becomes sharper as γ increases. Fig. 3 shows $A(\zeta)$ for four combinations of n and γ .

The two families of D clusters studied in this paper are: [A], clusters with $\gamma = 10$ and $n = 0.15, 1$ and 5 , which were chosen to study the effects of varying the position of A_{\max} in sharply peaked distributions; [B], clusters with $n = 1$ and $\gamma = 1.1, 10$ and 20 , which were chosen to study the effect of varying the sharpness of the peak with fixed n . We refer below to these as the [A] and [B] families.

Fig. 4a displays the results for the [A] family. The dashed lines are the loci of maximal fractional binding energy, while the solid lines indicate the onset of dynamic instability. For temperatures $T_\infty \gtrsim 3$ there is very little difference in either the structure or dynamic stability of these clusters, but marked differences are apparent at lower temperatures. When $n = 0.15$ the binding energy curve does not appear to turn over and approach small values of z_c with decreasing T_∞ as happens with $n = 1$ and 5 . These turnovers occur at successively higher values of T_∞ as n increases. For $n = 0.15$ the stability and binding energy curves are close for all values of T_∞ but, for $n = 1$ and 5 , they depart on the cooler side of the turnover points. We are only confident that the stability results indicate the true stability picture on the warmer side of the turning points because for $n = 1$ and 5 these D clusters develop core-halo structures in a similar manner to ND clusters. Moreover, this process is accentuated as n increases. However, when n is as small as 0.15 , core-halo structures do not develop for small T_∞ , at least for clusters with $z_c \lesssim 0.65$. Consequently, the stability results for clusters with $n = 0.15$ and $\gamma = 10$ are probably accurate for the entire range of T_∞ shown in Fig. 4a.

Some dimensionless features of the [A] and [B] families, as well as of the ND clusters, are displayed in Fig. 5 as functions of T_∞ . In this figure, all clusters have $z_c = 0.54$, the full curves represent the central condensation $\Delta = \rho_c/\langle\rho\rangle$ and the dashed curves represent the dimensionless coordinate radius ξ_1 . Clusters with large Δ usually have large ξ_1 as well. As Fig. 5 indicates, for clusters with $n = 5$ and $\gamma = 10$, both Δ and ξ_1 increase rather dramatically with increasing T_∞ . In contrast with this, Δ and ξ_1 do not increase significantly for clusters with $n = 0.15$ and $\gamma = 10$.

We did not study any clusters with $\gamma = 10$ and $n > 5$ because of numerical difficulties. Since the parameter α is related to n and γ by $\alpha = n\gamma + 5$, it follows that we have $\alpha > 55$ when $\gamma = 10$ and $n > 5$. When α and μ are both large (i.e. for small T_∞) we have difficulty evaluating the expressions given in the Appendix for p , ρ and ρ_0 by the method of continued fractions. This difficulty arises from the last factor $\{1 - u\mu(1 - y^{\frac{1}{2}})/(\gamma + \mu)\}^{-\alpha}$ from the integrand in equation (A14), which increases extremely rapidly when the dummy variable of integration u approaches unity with

both $\alpha \gg 1$ and $\mu(1-y^2)/(\gamma+\mu) \approx 1$. The value $n = 5$ was about as large as we could manage with $\gamma = 10$.

Fig. 4b is a similar plot to Fig. 4a but for the [B] family; the clusters with $n = 1$ and $\gamma = 10$ being common to both families. There are marked similarities between Figs. 4a and 4b in that the low temperature clusters of the [B] family also show an increase in central condensation when γ is large. Some dimensionless features of specific models from the [B] family are shown in Fig. 5 for comparison with the other clusters. On the basis of the above stability and structural calculations, it seems unlikely that any D clusters belonging to either the [A] or [B] families can be dynamically stable for $z_c \gtrsim 0.6$.

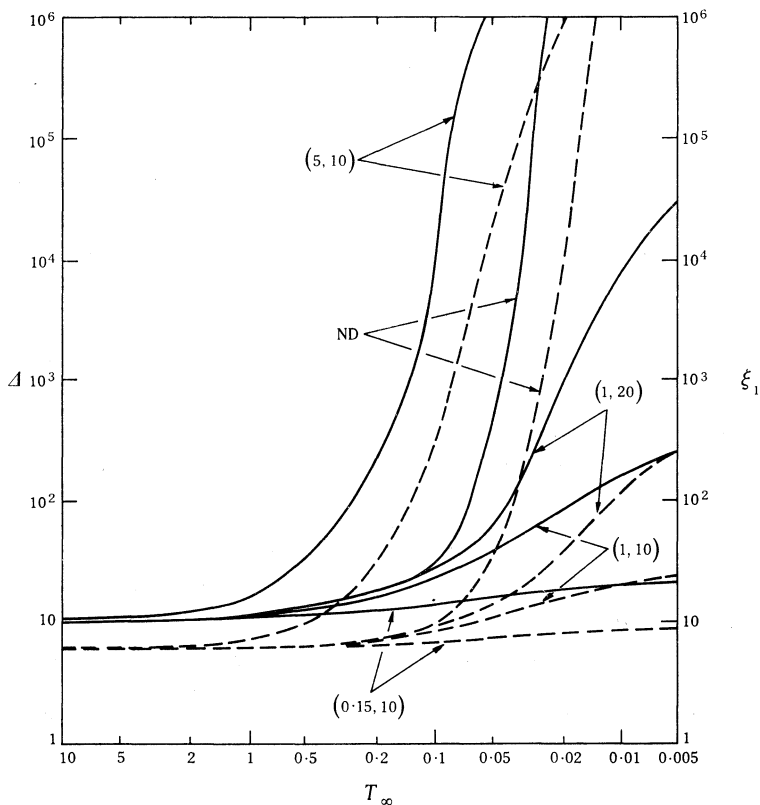


Fig. 5. Central condensation $\Delta = \rho_c/\langle\rho\rangle$ (full curves) and dimensionless coordinate radius ξ_1 (dashed curves) as functions of T_∞ for all D clusters considered here (except for $(1, 1.1)$) and for ND clusters. All clusters in this figure have $z_c = 0.54$, and the values of the parameters (n, γ) are indicated for the D clusters.

Correspondence Between D and ND Clusters

The D and ND clusters do not form a completely disjoint set because ND clusters can be obtained as a special limiting case of D clusters. For a fixed value of n , the form of $g(\zeta)$ in equation (3) approaches the delta function $\delta(\zeta - n)$ as $\gamma \rightarrow \infty$, provided the constant K is chosen so that

$$\int_0^\infty g(\zeta) d\zeta = 1.$$

The required value of K for this to be true is

$$K = \Gamma(n\gamma + 5) m_0^5 \gamma^{n\gamma+1} / \Gamma(n\gamma + 1).$$

Thus, if n remains finite in the limit $\gamma \rightarrow \infty$, we expect the dimensionless structure of D clusters to approach that of ND clusters. The fact that K must be specified in the process is irrelevant since the dimensionless structure equations (8a)–(8c) do not contain K . Also irrelevant to the result is the fact that

$$g(\zeta) \rightarrow \delta(\zeta - n) = m_0 \delta(m - nm_0)$$

instead of $g(\zeta) \rightarrow \delta(m - m_0)$, because the presence of n in the delta function argument only amounts to a redefinition of m_0 . Since this does not affect the dimensionless structure either, it is not necessary to have $n = 1$ in $\delta(m - nm_0)$.

The quantities $\rho_c / \langle \rho \rangle$ and ξ_1 for ND clusters are given for comparison with D clusters in Fig. 5. The D clusters with structures closest to ND clusters are those with $n = 5$ and $\gamma = 10$, and $n = 1$ and $\gamma = 20$, but neither of these sequences are close for the entire range of T_∞ in Fig. 5. Although all the D clusters that we calculated with $n = 1$ and $\gamma = 20$ had dimensionless structures agreeing to three significant figures with the dimensionless structures of ND clusters in the region of the z_c, T_∞ plane for which $z_c \lesssim 2$ and $T_\infty \gtrsim 8$, it appears that much smaller values of the ratio n/γ than we are able to use would be required to obtain similar agreement over the entire z_c, T_∞ plane.

Dimensional Properties of Isothermal Clusters

The discussion so far has concerned only dimensionless properties and features of the clusters. Before any *physical* quantities such as the total mass-energy, the radius or the number of stars can be calculated, a value for the scaling parameter K must be specified. However, from a computational point of view, it is more convenient to specify the total rest mass M_0 . This is equivalent to specifying K , since M_0 also acts as a scaling parameter for the isothermal clusters (Misner *et al.* 1973, p. 686). Once the dimensionless structure is calculated and M_0 is specified, the total mass-energy follows from $M = (1 - \mathcal{E})M_0$ and the coordinate radius follows from $R = (1 - \mathcal{E})M_0 \tau^{-1}$, where τ is the *dimensionless* ratio M/R given by the right-hand side of equation (18). For ND clusters the total number of stars N is given by $M_0 = Nm_0$, once the reference stellar rest mass m_0 is specified. In the case of D clusters this last relation is replaced by $M_0 = N\bar{m}$, where $\bar{m} = (\gamma n + 1)m_0/\gamma$ is the mean stellar rest mass. A further quantity of interest is the central number density of stars n_c . If we denote by η the dimensionless ratio $\xi_1^3/3 w(\xi_1)$ in equation (19), it follows that $n_c = \langle n \rangle \eta$ for both types of clusters, where $\langle n \rangle = 3N/4\pi R^3$. In terms of astrophysical units, R and n_c become

$$R = 4.81 \times 10^{-14} \tau^{-1} (1 - \mathcal{E}) (m_0/m_\odot) N \text{ pc}$$

and

$$n_c = 2.15 \times 10^{39} \tau^3 \eta^{-1} (1 - \mathcal{E})^{-3} (m_0/m_\odot)^{-3} N^{-2} \text{ pc}^{-3}$$

for ND clusters, where m_\odot is the solar rest mass.

A basic assumption underlying the theory behind the clusters discussed in this paper is that the effects of direct stellar collisions can be ignored. We can check the validity of this collisionless theory by comparing the mean time between collisions

for a typical star \mathcal{T}^c with the time taken for a star to travel once around the boundary of the cluster \mathcal{T}^o . If $\mathcal{T}^c \gg \mathcal{T}^o$, the collisionless theory is valid. Since $\mathcal{T}^o = 2\pi\tau^{-\frac{1}{2}}R$ we can write

$$\mathcal{T}^o = 9.86 \times 10^{-13} \tau^{-3/2} (1 - \mathcal{E})(m_0/m_\odot) N \text{ yr.} \quad (22)$$

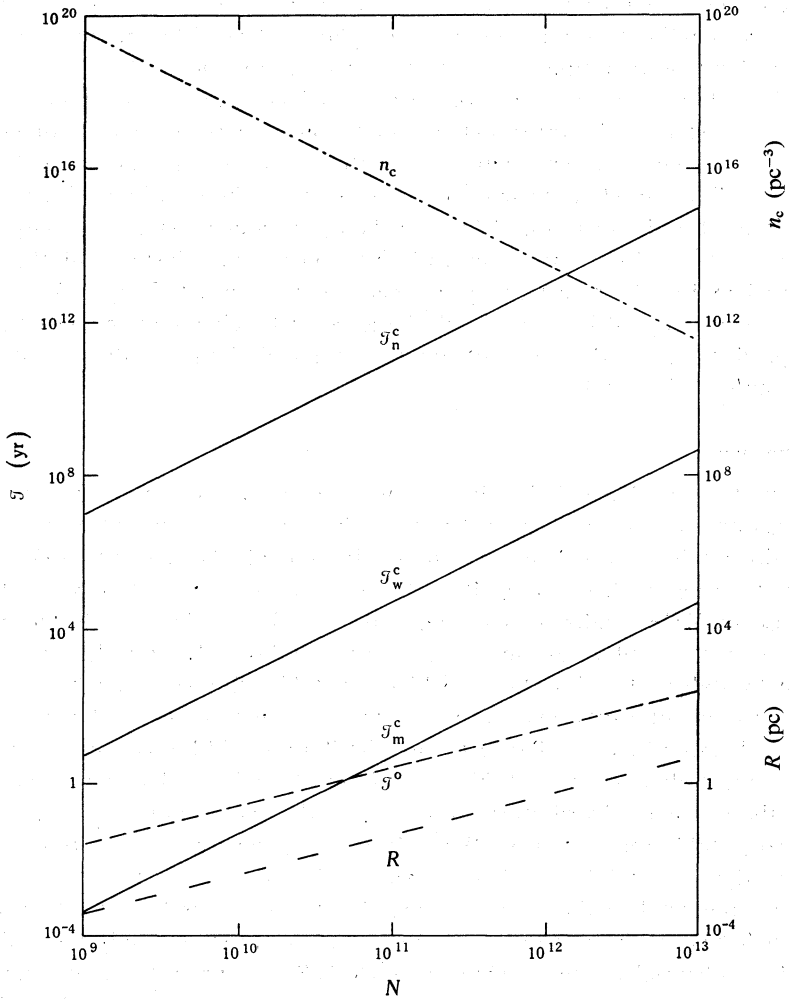


Fig. 6. Curves illustrating some physical properties of an ND cluster with $z_c = 0.490$ and $T_\infty = 0.295$ (corresponding to the point C' in Fig. 1) as functions of the total number of stars N . The mean time between stellar collisions \mathcal{T}^c is shown for clusters consisting of main sequence stars \mathcal{T}_m^c , white dwarfs \mathcal{T}_w^c and neutron stars \mathcal{T}_n^c , together with the time \mathcal{T}^o for a star to orbit once around the boundary of the cluster. Also shown are the central number density of stars n_c and the physical coordinate radius R .

For an estimate of \mathcal{T}^c we can use the Newtonian expression of Spitzer and Saslaw (1966, equation 16) which, in our notation, becomes (for ND clusters)

$$\mathcal{T}^c = 2.36 \times 10^{-25} \frac{\tau^{-7/2} (1 - \mathcal{E})(m_0/m_\odot)^3 (r/r_\odot)^{-2} N^2}{1 + 2.12 \times 10^{-6} \tau^{-1} (m_0/m_\odot) (r/r_\odot)^{-1}} \text{ yr,} \quad (23)$$

if r_{\odot} is the solar radius. From equations (22) and (23), the condition $\mathcal{T}^c \gg \mathcal{T}^o$ now entails

$$N \gg 4 \times 10^{12} \tau^2 (m_0/m_{\odot})^{-2} (r/r_{\odot})^2, \quad (24)$$

which is consistent with Fackerell (1968, p. 644).

For an ND cluster with $z_c = 0.490$, $T_{\infty} = 0.295$, $\tau = 0.109$ and $\eta = 10$ (i.e. a cluster corresponding to a point on the z_c, T_{∞} plane indicated by the dot C' in Fig. 1), Fig. 6 displays the quantities \mathcal{T}^o , \mathcal{T}^c , R and n_c as functions of N . The collision period \mathcal{T}^c is shown for three series of clusters, each containing a different population of solar mass stars. The three stellar populations comprise: main sequence stars with $r/r_{\odot} = 1$, white dwarfs with $r/r_{\odot} = 10^{-2}$, and neutron stars with $r/r_{\odot} = 1.5 \times 10^{-5}$. For the white dwarfs and neutron stars, the condition (24) is satisfied for all values of N shown in Fig. 6 but, for the main sequence stars, it is only satisfied for $N \gtrsim 3 \times 10^{12}$. By comparison with Newtonian star clusters, all the clusters represented in Fig. 6 are extremely compact, with radii satisfying $4.3 \times 10^{-4} \leq R \leq 4.3$ pc, and they all have extremely large central stellar number densities. The average stellar number densities $\langle n \rangle$ are also extremely large for these clusters since $\eta = 10$ implies $\langle n \rangle = 0.1 n_c$.

6. Conclusions

The method of Paper I for diagnosing dynamic instability in relativistic star clusters is quite successful when applied to isothermal clusters provided the particular clusters do not have core-halo structures. In general, the method works well for isothermal clusters with $\rho_c/\langle \rho \rangle \lesssim 10^3$. The results presented in this paper, together with those of KHK, indicate that there are very few isothermal clusters with no dispersion in the stellar rest mass which can be both dynamically and thermodynamically stable. The few clusters which are stable all have $z_c \approx 0.5$.

The structure of isothermal clusters with dispersion in the stellar rest mass is strongly influenced by the stellar rest mass distribution. Although we have not made an exhaustive study of clusters of this type, our results indicate that, with the particular form of the rest mass distribution considered in this paper, none of the clusters are dynamically stable for $z_c \gtrsim 0.6$. We unfortunately have no information regarding the thermodynamic stability of these dispersive clusters.

A more powerful method for studying the dynamic stability of relativistic star clusters will have to be developed before we can successfully study the stability of core-halo isothermal clusters. One of us (K.G.S.) is currently developing such a method based on a variational principle containing an arbitrary number of terms, instead of a single term as used in this paper.

Acknowledgment

One of us (K.G.S.) thanks the University of Sydney for the provision of a Post-graduate Research Studentship.

References

- Appell, P., and Kampé de Fériet, J. (1926). 'Fonctions Hypergéométriques et Hypersphériques. Polynômes d'Hermite' (Gauthier-Villars: Paris).
- Erdélyi, A. (1953). 'Higher Transcendental Functions', Vol. 1 (McGraw-Hill: New York).

Fackerell, E. D. (1966). Ph.D. Thesis, University of Sydney.
 Fackerell, E. D. (1968). *Astrophys. J.* **153**, 643.
 Fackerell, E. D. (1970). *Astrophys. J.* **160**, 859.
 Fackerell, E. D., Ipser, J. R., and Thorne, K. S. (1969). *Comments Astrophys. Space Phys.* **1**, 134.
 Ipser, J. R. (1969). *Astrophys. J.* **158**, 17.
 Katz, J., Horwitz, G., and Klapisch, M. (1975). *Astrophys. J.* **199**, 307.
 Khovanskii, A. N. (1963). 'The Application of Continued Fractions' (Translated by P. Wynn) (Noordhoff: Groningen).
 Misner, C. W., Thorne, K. S., and Wheeler, J. A. (1973). 'Gravitation' (Freeman: San Francisco).
 Picard, E. (1880). *Comptes Rendus* **90**, 1267.
 Spitzer, L., and Saslaw, W. C. (1966). *Astrophys. J.* **143**, 400.
 Suffern, K. G. (1976). Ph.D. Thesis, University of Sydney.
 Suffern, K. G., and Fackerell, E. D. (1976). *Astrophys. J.* **203**, 477.
 Wall, H. S. (1948). 'Analytic Theory of Continued Fractions' (Van Nostrand: Princeton).
 Zeldovich, Ya. B., and Podurets, M. A. (1965). *Astron. Zhur.* **42**, 963; English translation in *Sov. Astron. AJ* **9**, 742.

Appendix. Evaluation of p , ρ and ρ_0

Most of the results given in this appendix are taken from Fackerell (1966).

ND Clusters

In the case of ND clusters, the mass weighted distribution function $\chi(x)$ follows readily from equations (1) and (2) as

$$\chi(x) = \frac{2}{3}\pi KH(1-x^{\frac{1}{2}})\exp(-\mu x^{\frac{1}{2}}). \tag{A1}$$

Substituting equation (A1) into equations (5)–(7) then results in the following expressions for p , ρ and ρ_0 :

$$p = (8\pi K/15y^2)Y^{5/2}Z^{3/2}\exp(-\mu)\Phi_1(1, -3/2, 7/2; Y/Z, \mu Y), \tag{A2}$$

$$\rho = 3P + (8\pi K/3y)Y^{3/2}Z^{1/2}\exp(-\mu)\Phi_1(1, -1/2, 5/2; Y/Z, \mu Y), \tag{A3}$$

$$\rho_0 = (8\pi K/3)y^{-3/2}Y^{3/2}Z^{1/2}\exp(-\mu)\Phi_1(1, -1/2, 5/2; Y/Z, \mu Y) - (16\pi K/15)y^{-3/2}Y^{5/2}Z^{1/2}\exp(-\mu)\Phi_1(2, -1/2, 7/2; Y/Z, \mu Y). \tag{A4}$$

Here $Y = 1 - y^{\frac{1}{2}}$, $Z = 1 + y^{\frac{1}{2}}$, and Φ_1 denotes Humbert's confluent hypergeometric function in two independent variables whose integral representation is (Appell and Kampé de Fériet 1926, p. 127)

$$\Phi_1(a, b, c; x, y) = \frac{\Gamma(c)}{\Gamma(a)\Gamma(c-a)} \int_0^1 u^{a-1}(1-u)^{c-a-1}(1-xu)^{-b}\exp(yu) du. \tag{A5}$$

We employ the following numerical technique to evaluate the hypergeometric functions occurring in p , ρ and ρ_0 . For $x < 1$, the function $\Phi_1(1, b, c; x, y)$ has the following expansions in terms of generalized hypergeometric functions of a single

variable (Appell and Kampé de Fériet 1926, p. 127)

$$\Phi_1(1, b, c; x, y) = \sum_{n=0}^{\infty} \{(b)_n/(c)_n\} {}_1F_1(n+1, c+n; y)x^n \tag{A6a}$$

$$= \sum_{n=0}^{\infty} {}_2F_1(n+1, b, c+n; x) y^n/(c)_n. \tag{A6b}$$

We write the series (A6a) and (A6b) in the form

$$\Phi_1(1, b, c; x, y) = {}_1F_1(1, c; y) \sum_{n=0}^{\infty} S_n, \tag{A7a}$$

$$= {}_2F_1(1, b, c; x) \sum_{n=0}^{\infty} T_n, \tag{A7b}$$

where $S_0 = T_0 = 1$ and, for $n > 0$, S_n and T_n are defined recursively by

$$S_{n+1} = x \frac{b+n} {c+n} \frac{{}_1F_1(n+2, c+n+1; y)}{{}_1F_1(n+1, c+n; y)} S_n, \tag{A8a}$$

$$T_{n+1} = \frac{y} {c+n} \frac{{}_2F_1(b, n+2, c+n+1; x)}{{}_2F_1(b, n+1, c+n; x)} T_n. \tag{A8b}$$

The ratio of hypergeometric functions in equation (A8a) is most conveniently evaluated by using the continued fraction expansion (cf. Khovanskii 1963, p. 138)

$$\frac{{}_1F_1(n+2, c+n+1; y)}{{}_1F_1(n+1, c+n; y)} = \frac{c+n} {c+n} \frac{(c-1)y} {c+n-1} \frac{(n+2)y} {c+n+2} \frac{cy} {c+n+3} \\ + \frac{(n+3)y} {c+n+4} \frac{(c+1)y} {c+n+5} + \dots$$

To evaluate the confluent hypergeometric function ${}_1F_1(1, c; y)$ in equation (A7a) we use the following relation

$${}_1F_1(1, c; y) = \Gamma(c) y^{1-c} \exp(y) + (1-c) \Psi(1, c; y),$$

which is a special case of equation (7) of Erdélyi (1953, p. 275). Here $\Psi(1, c; y)$ is the integral

$$\Psi(1, c; y) = \int_0^{\infty} \exp(-yu)(1+u)^{c-2} du,$$

provided $\text{Re}(y) > 0$. This integral can also be expanded by a continued fraction expansion, the appropriate expansion in this case being (Wall 1948, p. 356)

$$\Psi(1, c; y) = \frac{1} {y} + \frac{2-c} {1} + \frac{1} {y} + \frac{3-c} {1} + \frac{2} {y} + \frac{4-c} {1} + \frac{3} {y} + \dots$$

The ratio of hypergeometric functions in equation (A8b) may be evaluated by Gauss's

continued fraction expansion (cf. Wall 1948, p. 337)

$$\frac{{}_2F_1(b, n+2, c+n+1; x)}{{}_2F_1(b, n+1, c+n; x)} = \frac{c+n}{c+n} \frac{b(c-1)x}{c+n+1} - \frac{(n+2)(c+n-b+1)x}{c+n+2} - \frac{(b+1)cx}{c+n+3} - \frac{(n+3)(c+n-b+2)}{c+n+4} - \dots \quad (A9)$$

The expression (A9) may also be used to evaluate ${}_2F_1(1, b, c; x)$ in equation (A16) below with the substitution $n = -1$. For $|y| \leq 3$ in equation (A5), it is most efficient numerically to use the expansion (A6b), but for $|y| > 3$ it is most efficient to use (A6a).

Finally, the rest mass density ρ_0 , which involves $\Phi_1(2, -1/2, 7/2; Y/Z, \mu Y)$, is calculated by means of the following recurrence relation

$$\Phi_1(a, b, c; x, y) = \{(c-1)/(a-1)\} \Phi_1(a-1, b, c-1; x, y) - \{(c-a)/(a-1)\} \Phi_1(a-1, b, c; x, y). \quad (A10)$$

This is an immediate consequence of the integral representation (A5).

D Clusters

When $g(m)$ is given by equation (3), the distribution function $\chi(x)$ becomes

$$\chi(x) = \frac{2}{6} \pi K (\gamma + \mu x^3)^{-\alpha} H(1 - x^3).$$

From this expression, the quantities p , ρ and ρ_0 are given by

$$p = (8\pi K/15y^2) Y^{5/2} Z^{3/2} (\gamma + \mu)^{-\alpha} F_1(1, -3/2, \alpha, 7/2; Y/Z, \mu Y/(\gamma + \mu)), \quad (A11)$$

$$\rho = 3P + (8\pi K/3y) Y^{3/2} Z^{1/2} (\gamma + \mu)^{-\alpha} F_1(1, -1/2, \alpha, 5/2; Y/Z, \mu Y/(\gamma + \mu)), \quad (A12)$$

$$\rho_0 = (8\pi K/3y^{3/2}) Y^{3/2} Z^{1/2} (\gamma + \mu)^{-\alpha} F_1(1, -1/2, \alpha, 5/2; Y/Z, \mu Y/(\gamma + \mu)) - (16\pi K/15y^{3/2}) Y^{5/2} Z^{1/2} (\gamma + \mu)^{-\alpha} F_1(2, -1/2, \alpha, 7/2; Y/Z, \mu Y/(\gamma + \mu)), \quad (A13)$$

where F_1 denotes Appell's hypergeometric function in two independent variables. The following integral representation

$$F_1(a, b, b', c; x, y) = \frac{\Gamma(c)}{\Gamma(a)\Gamma(c-a)} \int_0^1 u^{a-1} (1-u)^{c-a-1} (1-xu)^{-b} (1-yu)^{-b'} du \quad (A14)$$

for $\text{Re}(c) > \text{Re}(a) > 0$ is taken from Picard (1880).

In the present case, we may use the expansion (Appell and Kampé de Fériet 1926, p. 15)

$$F_1(1, b, b', c; x, y) = \sum_{n=0}^{\infty} \{(b)_n/(c)_n\} {}_2F_1(b', n+1, n+c; y)x^n, \quad (A15)$$

provided $|x| < 1$. We evaluate the series (A15) by expressing it in an analogous

form to the series (A7a), namely,

$$F_1(1, b, b', c; x, y) = {}_2F_1(1, b', c; y) \sum_{n=0}^{\infty} S_n, \quad (\text{A16})$$

where $S_0 = 1$ and, for $n > 0$,

$$S_{n+1} = x \frac{b+n}{c+n} \frac{{}_2F_1(n+2, b', c+n+1; y)}{{}_2F_1(n+1, b', c+n; y)}.$$

The continued fraction expansion (A9) can again be used to calculate the ratio of hypergeometric functions in equation (A16) as well as the function ${}_2F_1(1, b', c; y)$.

An examination of the integral representations (A5) for Φ_1 and (A14) for F_1 reveals that, as far as the parameters a , b and c of F_1 are concerned, F_1 satisfies an identical recurrence relation to equation (A10). This is used to calculate the hypergeometric function appearing in the second term of equation (A13).

Manuscript received 26 November 1975